ELSEVIER

Polymer 41 (2000) 1497–1505

polymer

Simultaneous measurements of small- and wide-angle X-ray scattering during low speed spinning of poly(propylene) using synchrotron radiation

R. Kolb[a,*], S. Seifert[b], N. Stribeck[b], H.G. Zachmann[b]

[a]*Exxon Research and Engineering Company, Annandale, NJ 08801, USA*
[b]*Institut für Technische und Makromolekulare Chemie, University of Hamburg, Hamburg, Germany*

Abstract

Simultaneous measurements of small- and wide-angle X-ray scattering (SAXS and WAXD) were performed during the melt spinning of isotactic poly(propylene). The extruder assembly was mounted on a platform, which could be moved horizontally and vertically allowing variations of the measuring point between distances of 28 and 90 cm from the spinneret. The SAXS and WAXD pattern were taken simultaneously with two two-dimensional detectors. Additionally, the fiber diameter profile was measured. The development of the crystallization and the orientation of the crystallites were studied as a function of the distance from the spinneret. The wide-angle data revealed that highly oriented crystals grow out of an apparently unoriented amorphous matrix. Moreover, the orientation of the crystallites was found to be constant along the spin line. Both crystalline WAXD and SAXS peaks were found to occur at the same distance from the spinneret within the resolution of the apparatus. A comparison of WAXD and SAXS shows that the crystallization and the formation of a superstructure follow the same kinetics.

Keywords: Small- and wide-angle X-ray scattering; Poly(propylene); Melt spinning

1. Introduction

One of the most common ways to produce polymer fibers is the melt spinning process. The formation of fibers involves melting of the polymer, extrusion of the melt through a spinneret and, after cooling along the spin line, winding the resulting fiber on a roll. Melt spinning of fibers is a process, which imposes uniaxial deformation on the fiber while it is cooled down rapidly. Therefore, polymer crystallization, if any, occurs in a complex non-isothermal way and, because of the varying temperature along the spin line, under varying stress conditions. Because the properties of the final fiber are strongly influenced by the manufacturing conditions itself, it is necessary to better understand the development of the fine structure in order to optimize the industrial process of fiber spinning. Thus, there is a great commercial and scientific interest to investigate the structure forming process of fibers. On-line measurement of X-ray scattering during melt spinning is a powerful tool to reveal the structure development and has been performed extensively [1–9]. The first successful on-line measurements of structure development by means of a wide-angle diffraction have been performed by Katayama et al. [10]. They have investigated the development of crystallization and orientation of the polymer fiber during spinning of poly(propylene). Spruiell and White have done on-line wide-angle X-ray diffraction (WAXD) measurements on the same polymer using a rotating copper anode [3]. Their results show an increase in the crystallization rate with the spinning speed. The first small-angle scattering measurements using synchrotron radiation during spinning have been performed on poly(vinylidene fluoride) by Teidge et al. [5,11] and on poly(propylene) by Teidge [12]. These authors found that discrete small-angle scattering appears at a shorter distance from the die than the wide-angle diffraction peaks. They concluded that the small-angle X-ray scattering (SAXS) technique is more sensitive to structural changes than the WAXD. Ryan et al. performed simultaneous measurement of WAXD and SAXS during tape extrusion on iPP [13,14]. They found that SAXS patterns develop before the wide-angle reflections, and explained this with the presence of density fluctuations in the amorphous melt prior to crystallization.

The goal of this paper is a detailed study of the structure development of isotactic poly(propylene) during spinning at low take-up velocities. In particular, simultaneous real-time investigations of SAXS and WAXD using synchrotron radiation and measurements of the fiber diameter along the spin line were performed at varying spinning conditions.

* Corresponding author. Tel.: +1-908-730-2970; fax: +1-908-730-3314.
E-mail address: rkolb@erenj.com (R. Kolb)

0032-3861/00/$ - see front matter
PII: S0032-3861(99)00288-8

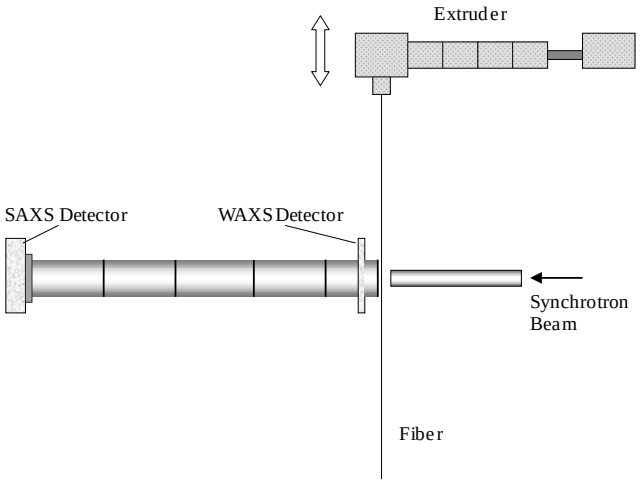

Fig. 1. The experimental set-up for simultaneous measurements of SAXS and WAXD during spinning.

The WAXD measurements provide information about the crystallization rate, the onset position of crystallization and the development of the crystallite orientation. The SAXS investigations reveal the development of the shape and the size of the polymer superstructure.

2. Experimental

2.1. Material

Isotactic poly(propylene) El Paso X® from Huels, Germany was used for extrusion. This polymer had a molecular weight of $M_w = 300\,000$ g/mol and a molecular weight distribution of $M_w/M_n = 7$. The melting temperature was 161°C. Before extrusion, the polymer was dried in vacuum at 100°C for 12 h.

2.2. Synchrotron facility

Measurements were performed at the polymer beamline at the Hamburg Synchrotron Radiation Laboratory (HASYLAB) at DESY in Hamburg using the double focusing camera of the polymer beamline A2 [15]. The primary beam intensity was measured by an ionization chamber and the scattering intensity was normalized by dividing it by the intensity of the primary beam.

2.3. Extrusion set-up

A single screw extruder manufactured by Brabender, Germany was used. The screw had a diameter of 20 mm and a length of 280 mm. A connected metering pump provided a constant mass throughput. The polymer pressure was controlled between the screw and the metering pump, and additionally between the metering pump and the spinneret. The extruder contained four heating zones. Each zone was controlled independently. Three zones were used to heat the extruder barrel and one zone to heat the spin block. Additionally, the spinneret could also be heated independently.

In order to measure the scattering of the fiber at various distances from the spinneret, the whole extruder assembly must be moved up and down, as the synchrotron beam is fixed. Therefore, the extruder assembly was mounted on a platform, which could be moved vertically and horizontally with the help of stepper motors, allowing variations of the measuring point between distances of 28 and 90 cm from the spinneret. The spinning experiments were performed at take-up speeds between 5 and 150 m/min using a winder from Erdman, Germany.

2.4. X-ray detection

As the polymer chains in the fiber are presumed to be oriented, anisotropic scattering patterns were expected. Therefore, two-dimensional detectors were necessary. To detect the scattering, phosphor imaging-plate devices were used as two-dimensional area detectors. The imaging-plate detecting the wide-angle diffraction had a hole of 14 mm in diameter in the center, so that the primary beam and the scattering at very small angles could pass. In this way, it became possible to detect the small-angle and the wide-angle diffraction simultaneously, with two two-dimensional detectors. To minimize the background scattering, the whole distance between the fiber and the detectors was evacuated. Fig. 1 shows schematically the experimental set-up. The air gap between the outlet of the primary beam and the first vacuum recipient was as small as 4 mm.

2.5. Degree of crystallinity and crystalline orientation

After taking an average over the azimuthal angle, the degree of crystallinity was determined from WAXD patterns by fitting an amorphous halo. The pattern of the amorphous halo was obtained during spinning at lower distances from the spinneret, where no crystallization occurs. Assuming a rotational symmetry of the specimen, the degree of crystallization is given by

$$x_c = \frac{\int_0^{\pi}\int_{s0}^{s1} I_c(s,\vartheta)s^2 \sin\vartheta \, ds \, d\vartheta}{\int_0^{\pi}\int_{s0}^{s1} I(s,\vartheta)s^2 \sin\vartheta \, ds \, d\vartheta}$$

where I_c is the integrated intensity of the crystal reflections and I represents the scattering intensity of both the amorphous and the crystalline part.

The azimuthal distributions of the 110, 040, and 130 reflection of the monoclinic α-form have been used to calculate the Hermans' orientation function, f, by applying the Wilchinsky method [16–20]. The factor f indicates the orientation of the polymer chains with respect to the fiber axis. f is defined in such a way, that the orientation function is unity for chains parallel to the fiber axis, equal to -0.5 if

Table 1
Temperature distribution of the different heating zones in the extruder

T_D (°C)	$T_{spin\ block}$ (°C)	$T_{zone\ 3}$ (°C)	$T_{zone\ 2}$ (°C)	$T_{zone\ 1}$ (°C)
210	200	190	180	175
225	215	195	180	175
240	230	215	190	180
270	260	245	215	190
300	290	270	235	200

the chains are aligned perpendicular to the fiber axis and 0 if the polymer chains are distributed randomly.

2.6. Small-angle scattering

The relative small-angle invariant, Q, was calculated from

$$Q = 4\pi \int\int I(s_r, s_z) s_r \, ds_r \, ds_z.$$

The determination of Q was complicated by several factors including a continuous change of the fiber diameter and a temperature decrease along the spin line. The decrease of the fiber diameter was corrected using the on-line measurement of the diameter profile as described below. The change of the electron density difference between the amorphous part, ρ_a, and the crystalline part, ρ_c, due to temperature decrease along the spin line was neglected. The long period, l_p, was determined from the maximum of the meridional reflection after Lorenz correction.

2.7. Measurement of the fiber diameter

On-line measurements of the fiber diameter were performed in two different ways:

Direct method
During spinning, the fiber was filmed and recorded by means of a CCD-camera in connection to a video recorder.

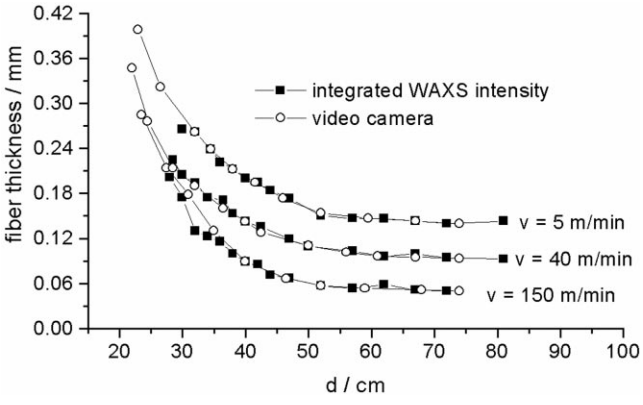

Fig. 2. The fiber diameter profile along the spin line at two take-up velocities, as measured directly by means of a video camera, and indirectly using the method of the integrated wide-angle diffraction intensity ($T_C = 210$°C).

After calibration, the fiber diameter was calculated from the average of 20 still-film pictures of the video film at each distance.
Relative method
The total intensity of the wide-angle diffraction pattern of the fiber was used as a relative value of the scattering volume. The scattering power, s, of isotactic poly(propylene) depends in the wide-angle region ranging from 1 to 3 on the scattering volume only [21]. It is independent from the orientation and the degree of crystallinity of the polymer chains as demonstrated by Ruland [21,22]. Therefore, the integrated WAXD intensity can be used to determine the fiber diameter. Advantages of this method include that the fiber diameter is measured simultaneously, with the wide-angle and small-angle scattering. Moreover, one single picture contains the information about the crystallinity and the orientation of the polymer chains, as well as of the fiber diameter.

2.8. Procedure

The X-ray scattering was measured as a function of the distance from the spinneret, d. The extrusion rate for all experiments was 0.6 m/min.

During the spinning experiments, three experimental parameters were changed.

1. The extrusion temperature at the die, T_D, was varied between 210 and 300°C. The gradients in the extruder at the various die temperatures are shown in Table 1. The temperatures of the four heating zones were changed according to the temperature of the die.
2. The take-up velocity, v, was changed between 5 and 150 m/min.
3. The distance from the spinneret, d, was varied from 28 to 90 cm.

3. Results and discussion

3.1. Fiber diameter

The measurements of the fiber diameter were used to determine whether or not a necking takes place. Additionally, the fiber diameter measurements were utilized to correct the small-angle scattering data regarding the scattering volume. Fig. 2 shows three examples of the fiber diameter profile along the spin line at different take-up velocities, as measured by means of the direct and the relative method. The extrusion temperature, T_D, was 210°C. The diagram shows very clearly that the diameter decreases continuously along the spin line. This indicates that no defined necking occurs. Moreover, a comparison of the two sets of curves proves that the method of the total intensity of the wide-angle diffraction is an appropriate measure of the fiber diameter. A variation of the temperature T_D, from 210 to 300°C at a given take-up velocity, influences the diameter profile practically not as shown in Fig. 3.

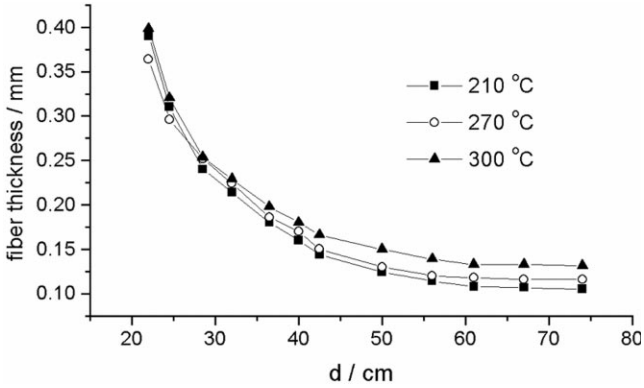

Fig. 3. The fiber diameter profile at three different temperatures, as calculated from the integrated wide-angle scattering intensity ($v = 40$ m/min).

3.2. Wide-angle X-ray diffraction

Fig. 4 shows the development of the WAXD at different distances, d, from the spinneret. At a distance of $d = 30$ cm, one can see an isotropic amorphous halo. At $d = 45$ cm, the WAXD pattern shows very weak reflections, which are oriented. The crystallization begins at this distance. The WAXD patterns further down the spin line, at $d = 60$ and 80 cm, respectively, show an increase in the reflection intensity, which is due to further crystallization of the polymer. The azimuthal width of the reflections is nearly constant along the spin line. The two-dimensional scattering patterns show that oriented crystals grow out of an apparently unoriented amorphous matrix. Moreover, the orientation of the crystallites does not change along the spin line.

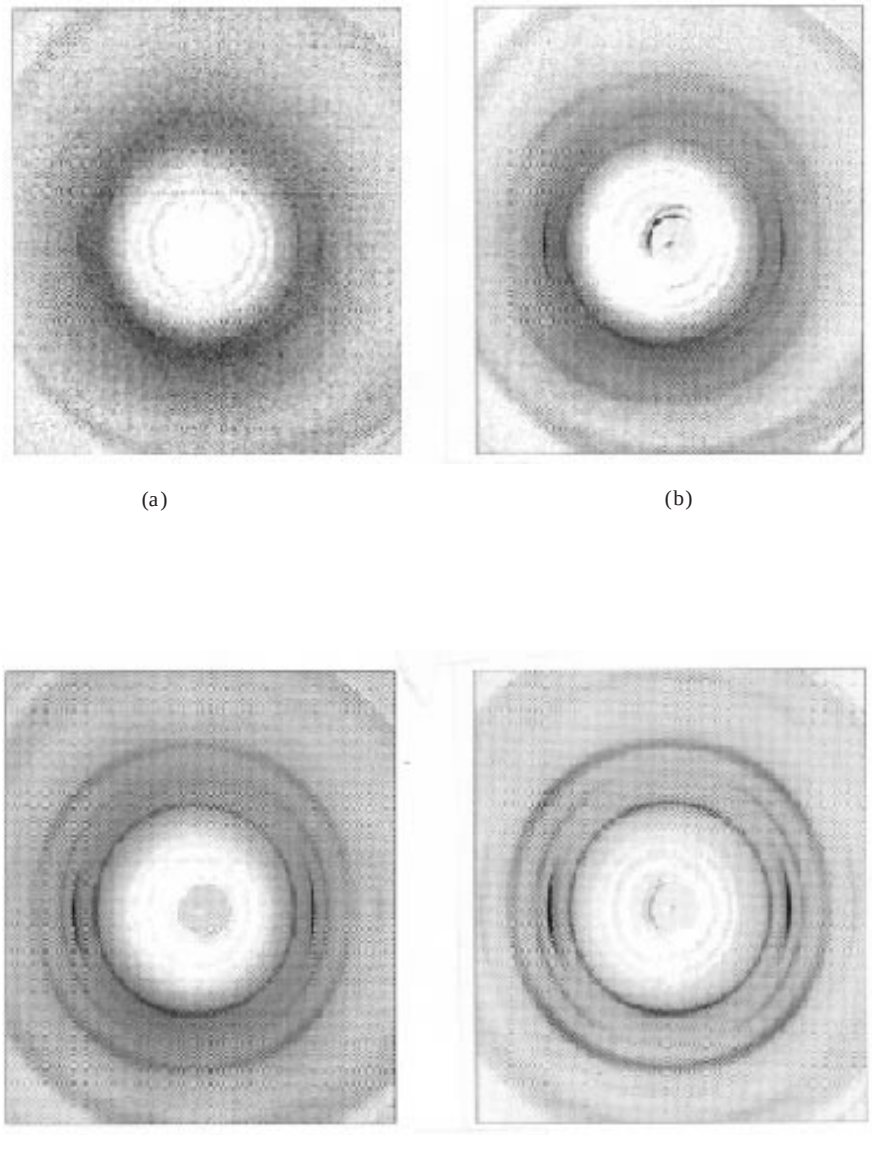

Fig. 4. The development of the wide-angle diffraction during spinning of isotactic poly(propylene) at: (a) 30; (b) 45; (c) 60; and (d) 80 cm. ($T = 210$°C; $v = 40$ m/min).

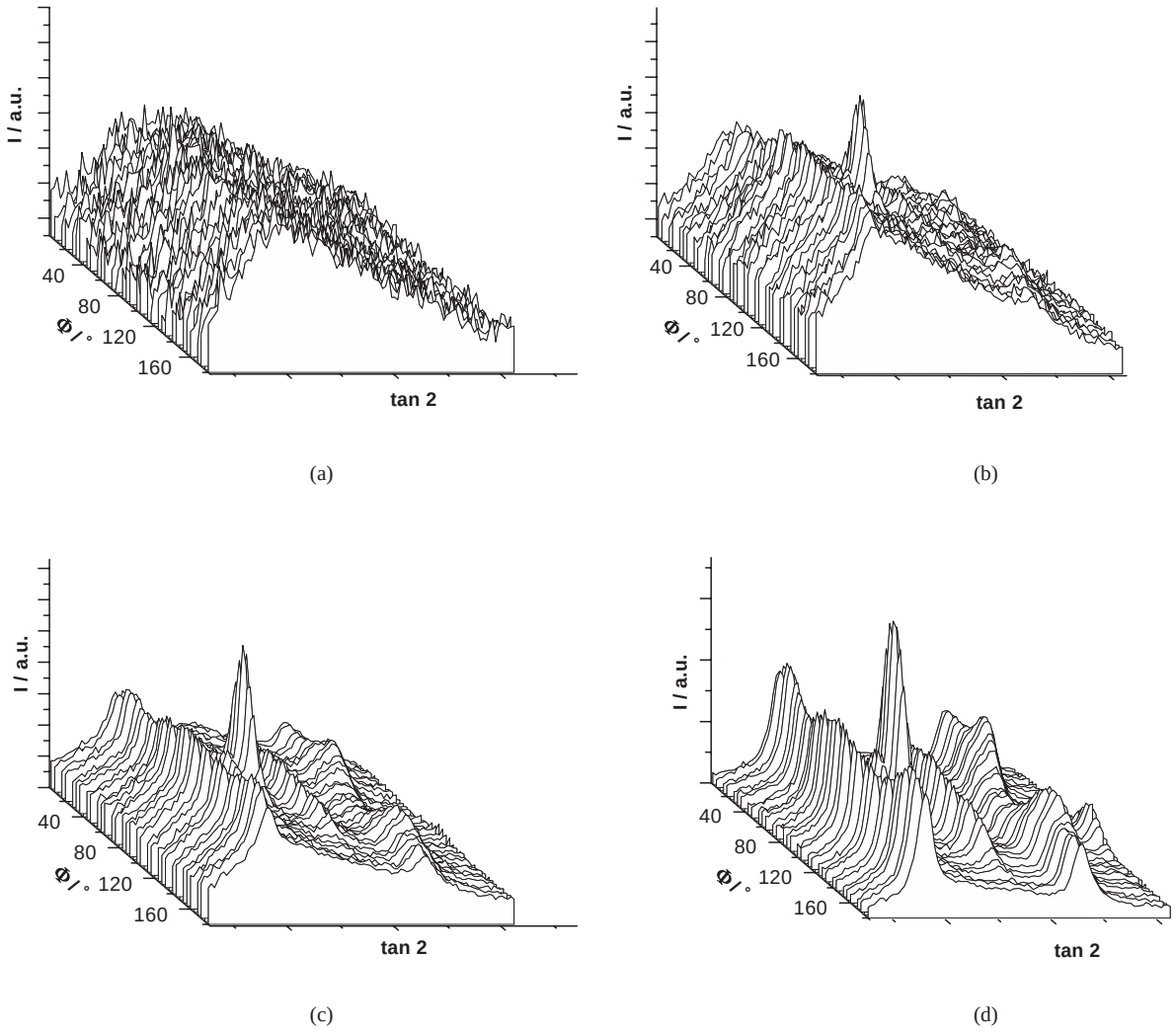

Fig. 5. The radial cuts through the two-dimensional wide-angle patterns (Fig. 4). The intensities were normalized.

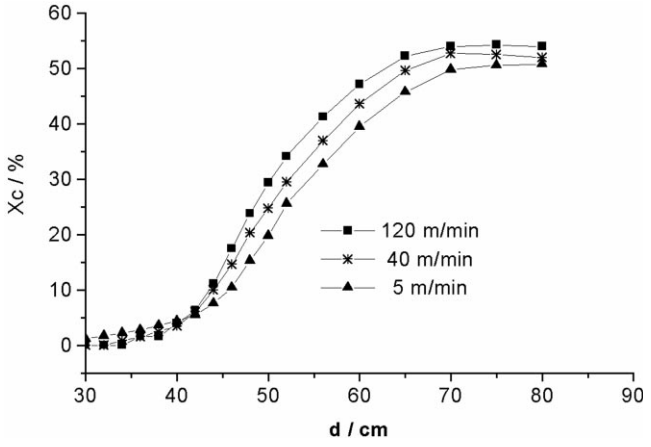

Fig. 6. The degree of crystallinity, x_c, as a function of the distance from the spinneret at 120, 40 and 5 m/min.

These results are in good agreement with previous investigations by Cakmak and Zachmann [5].

Fig. 5 shows radial cuts through the two-dimensional wide-angle patterns at different azimuthal angles ranging from $\phi = 0–180°$. Fig. 5(a) shows a clean amorphous halo at $d = 30$ cm, which indicates that the polymer chains are completely unoriented. Moreover, this kind of picture illustrates very clearly that highly oriented crystals grow out of the unoriented amorphous matrix.

Fig. 6 shows the degree of crystallinity, x_c, as a function of the distance, d, from the spinneret at three different take-up velocities ($T_D = 210°C$). The crystallization starts at a distance of 40 cm and reaches its final value at a distance of about 80 cm. The degree of crystallinity of the final fiber increases slightly with the take-up speed as can be seen in Fig. 7. The onset position of crystallization, x_p, moves slightly towards a shorter distance from the spinneret as the take-up speed increases. However, this change of x_p is insignificant.

Interestingly, for take-up velocities up to 150 m/min, the

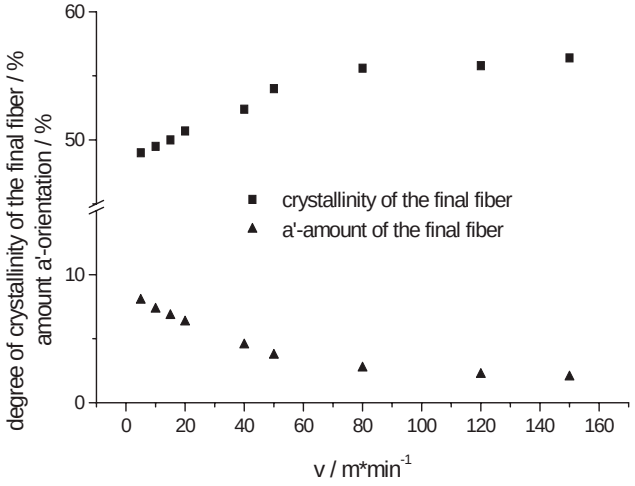

Fig. 7. The degree of crystallinity of the final fiber at different take-up velocities and the amount of a'- to c-axis oriented crystals in the final fiber as a function of the take-up velocity.

whole crystallization process occurs at distances between 30 and 90 cm from the spinneret ($T_D = 210$°C). The window in which crystallization takes place seems to be independent of the take-up velocity. Therefore, according to Fig. 6, it is clear that the crystallization velocity increases with the take-up speed. The non-isothermal crystallization process is mostly governed by the cooling rate and the stress. As the take-up speed increases, a volume element of the fiber moves faster to a given distance and has less time to crystallize. On the other hand, the stress increases with the take-up speed, which leads to a higher crystallization rate. For a given temperature, both parameters seem to change with the take-up velocity in such a way that the effect of the higher velocity of the fiber is just compensated by the higher stress, and the crystallization starts at about the same distance. Moreover, due to the higher crystallization rate,

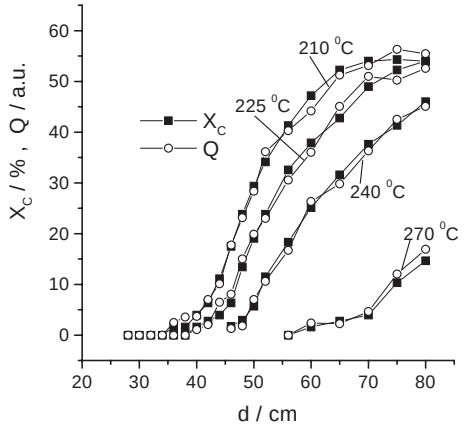

Fig. 8. The degree of cryztallinity, x_c, and the small-angle invariant, Q, as a function of the distance from the spinneret for four extrusion temperatures ($v = 40$ m/min). The intensities of the small-angle invariant were normalized.

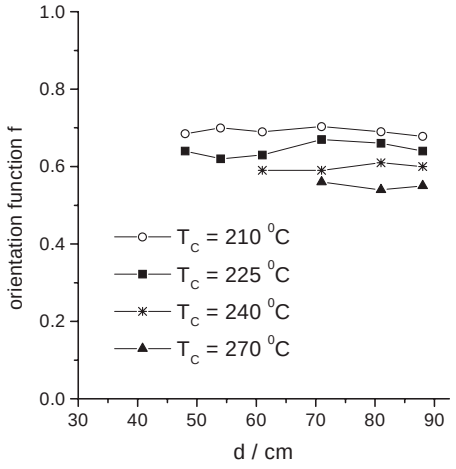

Fig. 9. Hermans' orientation function, f, as a function of the distance from the spinneret at different take-up velocities, v ($T_D = 210$°C).

the whole crystallization is completed at a distance of about 100 cm from the spinneret.

Fig. 8 shows the degree of crystallinity, x_c, and the small-angle scattering invariant, Q, as a function of the distance from the spinneret at four extrusion temperatures ranging from 210 to 300°C ($v = 40$ m/min). As the temperature increases, the onset position of crystallization, x_p, moves away from the spinneret. A comparison with the fiber diameter profile in Fig. 3 shows that the beginning of the crystalline solidification has no influence on the diameter profile of the fiber, and is not accompanied by a necking process.

Fig. 9 shows the Hermans' orientation function, f, as a function of the distance from the spinneret at four take-up velocities, v, ($T_D = 210$°C). The orientation function, f,

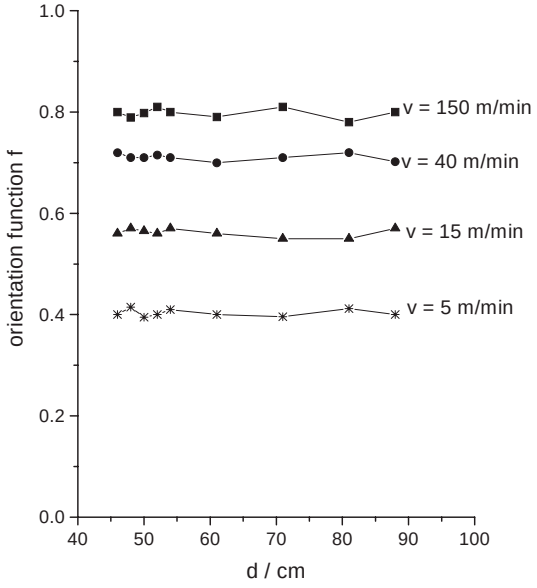

Fig. 10. Hermans' orientation function, f, as a function of the distance from the spinneret at different extrusion temperatures ($v = 40$ m/min).

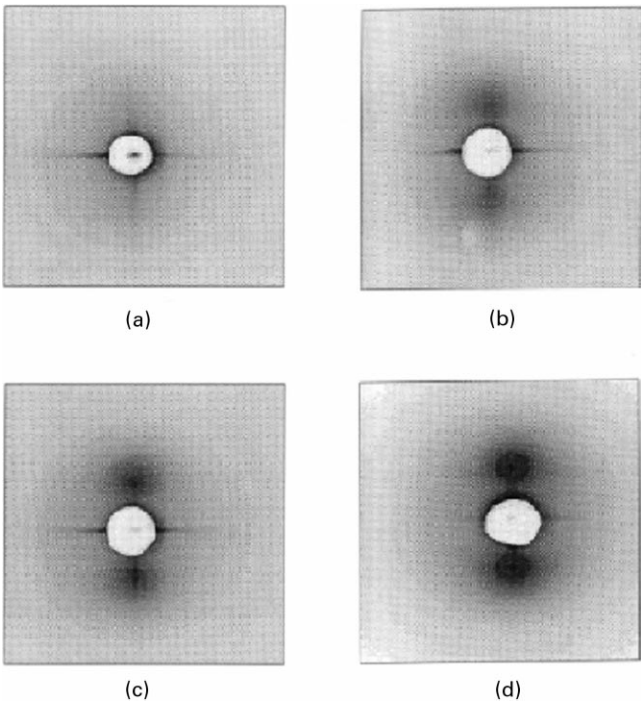

Fig. 11. The small-angle scattering patterns at different distances from the spinneret: (a) 30; (b) 45; (c) 60; and (d) 80 cm ($v = 40$ m/min; $T = 210$°C).

increases as the take-up speed increases, but is constant along the spin line for each take-up velocity. Fig. 10 represents f as a function of the distance from the spinneret at different extrusion temperatures ($v = 40$ m/min). Increasing the extrusion temperature with other variables unchanged, results in a lower orientation of the fiber. Similar results have been obtained by Spruiell and White [3]. However, the orientation does not change along the spin line. In each case, the orientation function, f, of the final fiber, is identical with the value obtained during spinning.

For take-up speeds up to 150 m/min, the orientation of the crystallites seems to be constant along the spin line for a wide variety of extrusion parameters. It must be concluded that the nucleation process of the crystallization determines the degree of crystalline orientation. It has been proposed earlier that prior to crystallization, a very small amount of highly elongated chain segments is present in the melt [7,12]. These few regions of oriented polymer chains act as nuclei for the crystallization, because of their higher order and higher density. The average orientation of these crystal nuclei increases with the take-up velocity because of the higher stress. After this nucleation phase, the crystallization itself occurs by a volume filling mechanism, involving chain folding out of the amorphous phase.

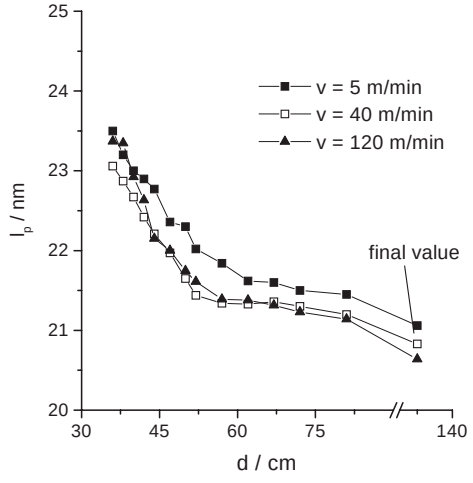

Fig. 12. The long period, l_p, versus the distance from the spinneret for three different extrusion temperatures.

As can be seen in Figs. 4 and 5, the iPP crystallizes in its α modification. The WAXD patterns further shows splitting of the 110 reflection into equatorial and meridional components. The equatorial maximum is due to the presence of c-axis oriented crystals and the meridional maximum to a^*-axis oriented crystals, respectively. These a^*-axis oriented crystals have been widely described in literature and attributed to lamellae branches that grow from the c-oriented parent lamellae. The a^*-axis of these branches point toward the fiber axis [10,23–27]. A careful examination of the X-ray patterns shows that the ratio of a^*- to c-axis oriented crystals is constant along the spin line. Furthermore, the a^*-axis crystals grow at the same rate as the c-axis oriented crystals. Similar to the orientation of the crystallites, the nucleation seems to be a critical step in the formation of this bimodal orientation. However, as the take-up speed increases, the ratio of a^*- to c-axis oriented crystals decreases. Fig. 7 shows the ratio of a^*- to c-axis oriented crystals as a function of the take-up velocity.

3.3. Small-angle X-ray scattering

The small-angle scattering was measured simultaneously with the WAXD to clarify the question, whether either a diffuse or a discrete SAXS occurs before crystal reflections can be observed.

Fig. 11 shows four small-angle scattering patterns at different distances from the spinneret ($T = 210$°C; $v = 40$ m/min). The pictures represent the raw data without background correction. The strong scattering at the equator is due to guard slits. Fig. 11 represents the typical pattern of a lamellae two-phase system, where the surface of the lamellae is oriented perpendicular to the fiber direction. The pictures indicate the presence of the lamellae two-phase system even from the very beginning of the crystallization. It can be concluded that the polymer chains crystallize by chain folding out of the amorphous phase.

The SAXS patterns in Fig. 11 correspond to the wide-angle patterns in Fig. 4. The picture obtained at a distance of $d = 30$ cm (Fig. 11(a)) shows no small-angle scattering. One can see an isotropic amorphous halo on the corresponding WAXD-picture (Fig. 4(a)).

As can be seen in Fig. 4(b), crystallization takes place at a

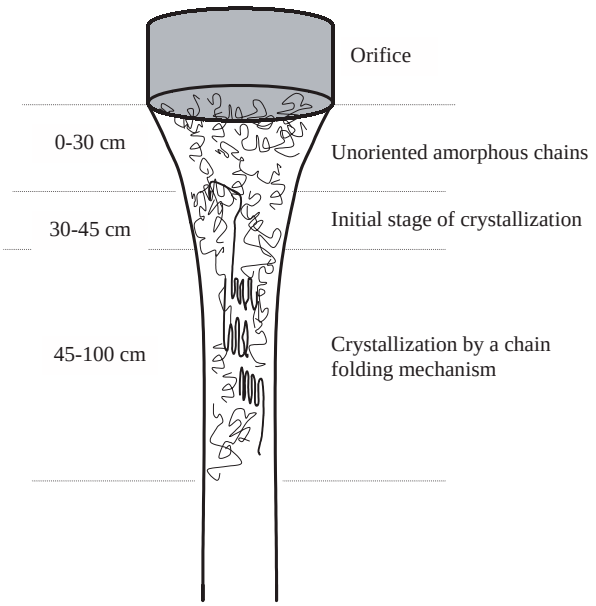

Fig. 13. Schematic illustration of crystallization in isotactic poly(propylene) fibers during low speed spinning.

distance of 45 cm. The corresponding SAXS image in Fig. 11(b) shows two weak meridional reflections. The small- and the wide-angle diffractions occur at the same distance of the spinneret. The small-angle reflections become stronger with increasing distances from the spinneret due to further crystallization of the fiber. No diffuse SAXS was observed prior to the appearance of the meridional reflections suggesting that no large-scale density fluctuations are present in the melt. If these density fluctuations would occur as precursors for crystallization as proposed by Ryan et al. [13,14], then the signal arising from these density fluctuations is too small to be detected by our apparatus due to the very small scattering volume of one single fiber.

A comparison of the development of Q and x_c, as shown in Fig. 8, proves that both have the same kinetics. Similar to the onset position of crystallinity, the appearance of the small-angle scattering shifts at higher temperatures away from the die.

Fig. 12 shows the development of the long period, l_p, versus the distance from the die for three extrusion temperatures ($v = 40$ m/min). As can be seen very clearly, the long period decreases at higher distances from the spinneret. This decrease of l_p suggests that thinner lamellae grow as the crystallization process progresses. These thin lamellae may be inserted in the existing lamellae stacks or grow in the remaining amorphous regions. It is to be noted, however, that l_p approaches a constant value at a distance of 50 cm, whereas the crystallization continues, as can be seen in Fig. 8. The final value of l_p is slightly lower than the values observed during spinning. This can be explained by the different thermal expansion coefficient of the crystalline and the amorphous phases.

Fig. 13 summarizes the structure forming process during the low-speed spinning of isotactic poly(propylene). In the first phase, directly behind the spinneret, the molten polymer is elongated and the fiber diameter decreases quickly. In this region the polymer chains are completely unoriented, which could be due to the high temperature and the fast thermal relaxation of the chains. Therefore, the existing entanglements are not stable. As one progresses further down the spin line, the polymer is cooled down to a temperature, at which the chain mobility becomes very low and the thermal relaxation of the chain is so slow that the entanglements act as fixed net points. Consequently, a rubber-like elongation occurs accompanied by an orientation of the chains. These few regions of oriented polymer chains act as nuclei for the crystallization, because of their higher order and higher density. The orientation of these crystal nuclei is the reason why the growing crystallites are also oriented, even at the beginning of the crystallization. The crystallization itself occurs by chain folding of the previously amorphous material.

4. Conclusion

From the X-ray scattering data and the data of the fiber diameter the following was determined. It was shown that the molten amorphous phase is completely unoriented and highly oriented crystals grow out of an isotropic amorphous matrix. The orientation of these crystallites remains constant during crystallization. By measuring the WAXD and the SAXS simultaneously, it was shown that these reflections occur at the same distance of the spinneret. The small-angle data further show that a lamella superstructure containing folded polymer chains is formed. Measurements of the fiber revealed that no necking occurs.

Acknowledgements

The authors thank Prof. Ben Hsiao of the State University of New York for very helpful discussions and Ralph Doehrmann for excellent technical support. This research was carried out at the Hamburg Synchrotron Radiation Laboratory (HASYLAB) at DESY and was partly founded by the German Federal Ministry of Science and Technology under the contract number 05-5 GUHXB.

References

[1] Fung PYF, Orlando E, Carr SH. Polym Engng Sci 1973;13:295.
[2] Kitao T. J Polym Sci: Polym Phys Ed 1973;2:1091.
[3] Spruiell JE, White JL. Polym Engng Sci 1975;15:660.
[4] Nadella HP, Henson HM, Spruiell JE, White JL. J Appl Polym Sci 1977;21:3003.
[5] Cakmak M, Teitge A, Zachmann HG, White JL. J Polym Sci Part B: Polym Phys 1993;31:371.
[6] Bansal V, Shambaugh RL. Polym Engng Sci 1996;36(22):2785.
[7] Hirahata H, Seifert S, Zachmann HG, Yabuki K. Polymer 1996;37:5131.

[8] Hsiao BS, Kennedy AD, Leach R, Barton Jr, Harlow R, Ross R, Seifert S, Zachmann HG. ACS Polym Prep 1995;36(1):340.
[9] Samon MS, Schultz JM, Wu J, Hsiao B, Yeh F, Kolb R. Submitted for publication.
[10] Katayama K, Amano T, Nakamura K. Kolloid Z Z Polym 1968;226:125.
[11] Zachmann HG, Bark M, Teitge A, Röber S. In: Proceedings of the International Man-made Fibre Conference, Dornbirn, Austria.
[12] Teitge A. Dissertation, University of Hamburg, 1990.
[13] Ryan AJ. In: Proceedings of the Tenth International Conference on Small-angle Scattering (SAS-96), Campinas, Brazil, 1996.
[14] Ryan AJ. APS Bull 1997;43(1):454.
[15] Elsner G, Riekel C, Zachmann HG. Adv Polym Sci 1985;67:1.
[16] Hermans PH, Platzek P. Kolloid Z 1939;88:68.
[17] Hermans PH, Hermans JJ, Vermaas D, Weidinger A. J Polym Sci 1947;3:1.
[18] Hermans PH, DeBooys JJ. Kolloid Z 1939;88:73.
[19] Wilchinsky ZW. J Appl Phys 1960;31:1969.
[20] Alexander LE. X-ray diffraction methods in polymer science. New York: Wiley, 1969.
[21] Ruland W. Acta Cryst 1961;14:1180.
[22] Ruland W. Faser Textiltechnik 1960;15(11):533–7.
[23] Lenz J, Schurz J, Wrentschur E. Acta Polym 1984;35:74.
[24] Samuels RJ. J Polym Sci 1965;A3:1741.
[25] Owen AJ, Ward IM. J Macromol Sci (Phys) 1973;B7:417.
[26] Samuels RJ. Structured polymer properties. New York: Wiley, 1974.
[27] Clark ES, Spruiell JE. Polym Engng Sci 1976;16:176.